

UIQI: A Comprehensive Quality Evaluation Index for Underwater Images

Yutao Liu^{ID}, Ke Gu^{ID}, Senior Member, IEEE, Jingchao Cao^{ID}, Shiqi Wang^{ID}, Senior Member, IEEE, Guangtao Zhai^{ID}, Senior Member, IEEE, Junyu Dong^{ID}, Member, IEEE, and Sam Kwong^{ID}, Fellow, IEEE

Abstract—Due to the light absorption and scattering in waterbodies, acquired underwater images frequently suffer from color cast, blur, low contrast, noise, etc., which seriously degrade the image quality and affect their subsequent applications. Therefore, it is necessary to propose a reliable and practical underwater image quality assessment (IQA) model that can faithfully evaluate underwater image quality. To this end, in this article, we establish a novel quality assessment model for underwater images by in-depth analysis and characterization of multiple image properties. Specifically, we propose characterizing the image luminance, color cast, sharpness, contrast, fog density and noise to comprehensively describe the image quality to evaluate the underwater image quality more accurately. Dedicated features are elaborately investigated to characterize those quality-aware image properties. After feature extraction, we employ support vector regression (SVR) to integrate all the quality-aware features and regress them onto the underwater image quality score. Extensive tests performed on standard underwater image quality databases demonstrate the superior prediction performance of the proposed underwater IQA model to state-of-the-art congeneric quality assessment models.

Index Terms—Underwater image, image quality assessment (IQA), no-reference (NR), objective metric, statistical modeling.

I. INTRODUCTION

UNDERWATER imaging plays a vital role in underwater tasks, such as resource exploration, engineering construction, underwater rescue and biological research. However, the complex underwater environment and light scattering and

Manuscript received 27 December 2022; revised 22 May 2023; accepted 17 July 2023. Date of publication 2 August 2023; date of current version 2 February 2024. This work was supported in part by the National Science Foundation of China under Grants 62201538, 62076013, 62273011, and 62322302, in part by the Shandong Natural Science Foundation under Grant ZR2022QF006, and in part by the Beijing Natural Science Foundation under Grant JQ21014. The associate editor coordinating the review of this manuscript and approving it for publication was Dr. Balu Adsumilli. (*Corresponding authors:* Jingchao Cao; Junyu Dong.)

Yutao Liu, Jingchao Cao, and Junyu Dong are with the School of Computer Science and Technology, Ocean University of China, Qingdao 266100, China (e-mail: liuyutao@ouc.edu.cn; caojingchao@ouc.edu.cn; dongjunyu@ouc.edu.cn).

Ke Gu is with the Faculty of Information Technology, Beijing University of Technology, Beijing 100124, China (e-mail: guke@bjut.edu.cn).

Shiqi Wang and Sam Kwong are with the Department of Computer Science, City University of Hong Kong, Hong Kong SAR, China (e-mail: shiqwang@cityu.edu.hk; cssamk@cityu.edu.hk).

Guangtao Zhai is with the Institute of Image Communication and Information Processing, Shanghai Jiao Tong University, Shanghai 200240, China (e-mail: zhaiguangtao@gmail.com).

Digital Object Identifier 10.1109/TMM.2023.3301226

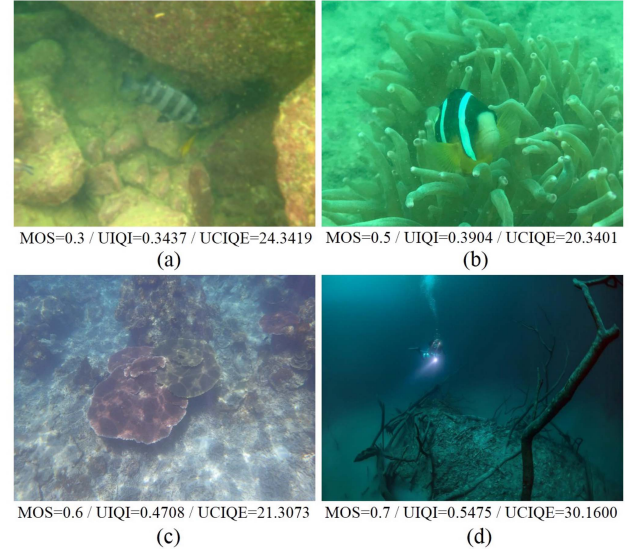


Fig. 1. Underwater images of different quality degradation conditions with their subjective MOS, UIQI and UCIQE [1] values. (a) blur; (b) color cast (greenish); (c) low contrast; (d) low luminance. It is clearly observed that the proposed UIQI values are more consistent with the ground-truth MOS values than the UCIQE values (The higher values of UIQI and UCIQE indicate the better image quality).

absorption through the water medium raise great challenges for acquiring a perfect-quality underwater image. For example, forward and backward scattering usually lead to blurry and low-contrast underwater images, as shown in Fig. 1(a) and (c), respectively. The different attenuation rates of different wavelengths of light in water usually make underwater images color cast. More specifically, red light has the highest attenuation rate, so underwater images are usually heavily greenish or bluish, as illustrated in Fig. 1(b). A dark underwater environment may lead to low-luminance underwater images (Fig. 1(d)). These undesirable effects severely damage the underwater image quality and restrict its subsequent applications. To monitor, control and improve underwater image quality, a credible underwater image quality evaluation method that quantifies underwater image quality accurately is urgently needed.

In the literature, according to the accessibility of the pristine ideal image, existing objective image quality assessment (IQA) methods can be classified into three types: full-reference (FR) [2] [3] [4], reduced-reference (RR) [5] [6] and no-reference (NR) or blind IQA approaches [7] [8]. Among them, FR or RR

IQA approaches apply full or partial information of the original pristine image to compute the image quality, while NR IQA methods evaluate the image quality without referring to its pristine counterpart. Since the underwater image lacks the original image, NR IQA provides the most suitable method for estimating the underwater image quality.

Although existing NR IQA approaches can be used to evaluate underwater image quality directly, most of them are designed for natural images (photographed over water), which have quite different degradation characteristics from underwater images, resulting in their prediction accuracy on underwater images being greatly limited [1]. Therefore, specialized underwater IQA methods must be developed to quantify the underwater image quality more precisely. To achieve this goal, several underwater IQA models have been proposed, such as the popular underwater color image quality evaluation metric (UCIQE) [1], underwater image quality measure (UIQM) [9] and CCF [10]. As the underwater image quality can be affected by many factors in practice, e.g., low or uneven luminance, color cast, blur, low contrast, fog, noise and their complex mixtures, characterizing a small number of image properties of the existing underwater IQA methods is still insufficient and ineffective for accurately evaluating the underwater image quality. A detailed analysis of existing underwater IQA models is given in Section II. More accurate and effective underwater IQA approaches are expected to be deeply explored.

In this article, we propose a novel underwater IQA method by analyzing multiple image properties. Specifically, we characterize the image overall luminance, luminance uniformity, sharpness, color cast, contrast, fog density and noise for evaluating underwater image quality, which is much more comprehensive than existing underwater IQA solutions for describing image quality. Dedicated features are carefully designed to represent these quality-aware properties felicitously. Support vector regression (SVR) is employed to regress the extracted quality-aware features to the image quality score. For convenience, we name our proposed quality model the underwater image quality index (UIQI). Broad image property analysis and proper feature design for characterizing the image properties make UIQI observably outperform state-of-the-art underwater IQA methods. As illustrated in Fig. 1¹, the proposed UIQI values are consistent with the MOS (mean opinion score) values. However, the UCIQE metric cannot achieve similar results. For example, Fig. 1(b) and (c) both have better quality than (a), while the UCIQE values of (b) and (c) are smaller than that of (a), which contradicts the ground-truth MOS values. These observations clearly demonstrate the superior ability of the UIQI in predicting underwater image quality.

We summarize the contributions of this article as follows:

- To the best of our knowledge, we make the first attempt to establish an underwater IQA method that measures underwater image quality from a much more comprehensive perspective than the existing underwater IQA approaches that investigate a small number of image properties for

quality evaluation. Specifically, we consider a broad range of essential image properties, i.e., the image luminance, sharpness, color cast, contrast, fog density and noise degree, to comprehensively characterize the underwater image quality.

- For each image property that affects the underwater image quality, combined with the characteristics of underwater imaging, we investigate the suitable means to measure it appropriately. Thus, dedicated features are elaborately designed to characterize the quality-aware image properties.
- Extensive experiments conducted on standard underwater image quality databases demonstrate that the proposed underwater IQA method achieves much better prediction performance in measuring underwater image quality than the state-of-the-art underwater IQA methods.

The rest of this article is organized as follows. In Section II, we overview the related IQA and specialized underwater IQA works. In Section III, we introduce the proposed underwater IQA approach in detail. Section IV gives the experimental results and necessary analysis. Finally, we draw conclusions in Section V.

II. RELATED WORKS

In this section, we give a detailed review of related works to this article, which include IQA methods for natural images and the existing specialized underwater IQA methods.

A. Image Quality Assessment Methods for Natural Images

Recent decades have seen plentiful preeminent IQA models proposed for measuring natural image quality. In FR IQA methods, the peak signal-to-noise ratio (PSNR) is widely adopted to represent image quality because of its simple computation and explicit physical meaning. Nevertheless, PSNR does not correlate well with subjective opinions on image quality [2]. To address this issue, Wang et al. proposed a milestone IQA measure, i.e., the structural similarity index (SSIM), which is based on the assumption that the human visual system (HVS) is highly adapted to extract image structural information for judging image quality. Later, some SSIM-type IQA measures, e.g., MS-SSIM [12], IW-SSIM [13], SC-SSIM [14], were developed from different concepts and further improved the prediction accuracy to some extent. Sheikh et al. proposed a visual information fidelity (VIF) index that characterizes the mutual information of the original and distorted images for quality evaluation [15]. Thorough tests confirm the excellent robustness of VIF for IQA. Zhang et al. exploited two low-level features, i.e., the gradient magnitude and phase congruency, to design a new feature similarity index (FSIM) [16]. By incorporating visual saliency features and a pooling strategy, Zhang et al. constructed a visual saliency-induced index (VSI) to quantify image quality [3]. A fast reliable IQA algorithm by fusing the macro- and micro-structures of the image was proposed, which achieves state-of-the-art prediction precision in the FR IQA field [17].

RR IQA methods predict image quality by referring to partial information of the original image. In [18], Soundararajan et al. computed the differences between the wavelet coefficient entropies of the reference and distorted images to characterize

¹All the example underwater images in this article are taken from the underwater image quality database [11].

image quality. Li et al. proposed an RR IQA algorithm by extracting the statistical features from the divisive normalization transformation (DNT) domain of the reference and distorted images [19]. Gao et al. proposed an RR IQA framework based on multiscale geometric analysis, which mimics the multichannel structure of HVS for quality perception [20]. Zhai et al. introduced the free-energy principle of brain theory into IQA and proposed an RR psychovisual quality model [6]. Based on Zhai's work, Liu et al. further employed sparse representation for approximating the internal generative model in the free-energy principle and proposed a free-energy principle and sparse representation-based index (FSI) for RR IQA [5], [21].

Early NR IQA models mainly exploited natural scene statistics (NSS) to establish IQA models based on the observation that NSS regularities tend to be modified by external distortions [22], [23]. For example, in [22], Mittal modeled the NSS regularities of the locally normalized luminance coefficients and extracted the quality-aware features for quality evaluation. Moorthy et al. [24] designed the NSS features of the wavelet coefficients of the image to predict image quality. In [25], Mittal et al. fitted the NSS features with the multivariate Gaussian (MVG) model on a set of pristine images, which served as the side information to deduce the image quality score. Zhang et al. enriched the NSS features from gradients, log-Gabor filter responses and color to improve the prediction performance [26]. Liu et al. designed NSS features to characterize the image structure, naturalness and perception for quality computation. In [27], Xu et al. exploited high-order statistical features to evaluate image quality. A highly efficient NR IQA model was proposed, which leverages the quality-aware NSS features extracted from the binary patterns of local image structures [28].

In recent years, deep learning technology in terms of the convolutional neural network (CNN) has developed rapidly and has achieved extraordinary success in computer vision tasks, such as image classification [29], object detection [30] and semantic segmentation [31], which spawned a batch of first-class NR IQA models. In [32], Kang et al. designed a CNN to learn discriminant features for quality estimation. In [33], Ma et al. generated a vast number of quality-discernable image pairs to learn an NR IQA method with RankNet. In [34], Kim et al. proposed a CNN-based NR image quality evaluator that narrowed the accuracy gap between FR IQA and NR IQA approaches. Bosse et al. [35] established a deeper network for both FR IQA and NR IQA, which jointly learned local quality and local weights in a unified framework. Su et al. [36] proposed a self-adaptive hypernetwork to blindly assess image quality. In [37], Zhang et al. developed a unified NR IQA model and a training strategy for evaluating the quality of images contaminated by both synthetic and realistic distortions.

B. Underwater Image Quality Assessment Methods

By analyzing the characteristics of underwater images, specialized underwater image quality evaluation methods are proposed to assess the quality of underwater images. A few representative works along this direction have been reported. Schechner et al. [38] employed image contrast as a quantitative

measure of underwater image quality. In [1], Yang et al. proposed an influential UCIQE metric, which linearly combines image chroma measurements, contrast and saturation in the CIELab color space. The human-visual-system-inspired underwater image quality measure (UIQM) is another widely adopted quality prediction model of underwater images, which is a combination of three independent measurements, i.e., underwater image colorfulness measure (UICM), underwater image sharpness measure (UISM) and underwater image contrast measure (UIConM) [9].

The CCF method was proposed by characterizing the colorfulness, contrast and fog density of underwater images [10]. Yang et al. [39] proposed a vectorial quality measure for underwater video, which consists of a discriminator C that distinguishes different marine habitats and a patch-based metric Q that predicts the image quality. An underwater image sharpness assessment method was proposed on the basis of the selective attenuation of color in water [40]. In [41], Li released an open framework for underwater IQA, which characterizes color cast and visibility degradation. In [42], Lu et al. conducted a quantitative analysis of the underwater image quality from the contrast-to-noise ratio, structure similarity and color distance. Recently, Tang et al. [43] investigated the sharpness, contrast and chroma measures and then combined them to infer the underwater image quality. Yang et al. performed underwater image quality evaluation by integrating the measurements of the contrast, colorfulness and sharpness of the underwater image [11]. Guo et al. evaluated the quality of enhanced underwater images by characterizing the underwater physics of underwater optical imaging and HVS-based attributes [44], [45].

Some deep learning-based underwater IQA methods have also been established. In [46], a generation-based joint luminance-chrominance underwater IQA model was constructed, which learns the effective feature representations in the chrominance and luminance domains of the image to evaluate the image quality. In [47], Fu et al. proposed a twice-mixing framework for underwater IQA that generates ranking images first and predicts the image quality with a Siamese network. In underwater image enhancement works, some underwater IQA approaches have been proposed for better assisting image enhancement. Guo et al. [48] built a URanker model based on the efficient convolutional image transformer, which is then used to supervise the underwater image enhancement module to obtain better image quality. Similarly, Wang et al. [49] proposed a simple yet efficient rank-based underwater IQA algorithm by training a Siamese network with the associated subjective MOS values. In [50], an underwater IQA network was constructed to generate a confidence map indicating the local perceptual quality of the underwater image, which is integrated to guide underwater image enhancement.

As stated before, the underwater image quality can be affected by many factors; however, the above underwater image quality prediction methods that mostly characterize a small number (no more than three) of image properties are still inadequate to accurately evaluate the underwater image quality. More accurate and comprehensive underwater IQA methods are worthy of further study.

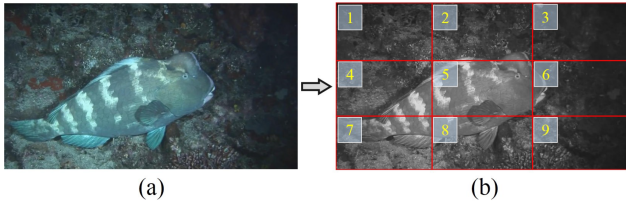


Fig. 2. Uneven-luminance underwater image and its partition for evaluating its luminance homogeneity. (a) underwater image whose MOS value is 0.5; (b) partition of (a).

III. THE PROPOSED UNDERWATER IMAGE QUALITY INDEX (UIQI)

In the proposed UIQI, we first characterize multiple underwater image properties, which are the image luminance, color cast, sharpness, contrast, fog density and noise, to describe the underwater image quality more comprehensively. For each image property, we exploit specific features to characterize it properly. Then, we employ SVR to regress all the quality-aware features to the image quality score. In the following, we introduce the processes of feature design and quality prediction in detail.

A. Characterization of Multiple Underwater Image Properties

1) *Luminance Evaluation*: Due to light absorption and the dark underwater environment, the acquired underwater images are possibly of insufficient luminance, which directly affects the image quality. Therefore, we first examine the overall luminance level of the underwater image for quality evaluation. Assume that the input underwater image is I . We transform I into its gray version, which only retains the luminance information of the image, denoted as I_g . Then, we calculate the mean value of I_g as:

$$l = \frac{1}{N} \sum_{i=1}^N I_g(i) \quad (1)$$

where l represents the mean value of I_g and N refers to the number of pixels in I_g . We employ $l/255$ as the quality-aware feature to evaluate the overall luminance level of I .

In addition to the overall luminance, the luminance homogeneity of an image is also an important index of the image quality. We show an uneven-luminance underwater image in Fig. 2(a) whose MOS value is 0.5 (1 indicates the best quality). The uneven luminance has an inevitable effect on the image quality. To evaluate the degree of luminance homogeneity of the underwater image, we divide the gray image I_g into nine blocks evenly, as illustrated in Fig. 2(b). We calculate the mean value of each block to estimate the overall luminance of each block, denoted by $m_i, i \in \{1, 2, \dots, 9\}$. Then, the difference between the maximum value and the minimum value in $\{m_1, m_2, \dots, m_9\}$ is computed to measure the luminance variation range of the image. The ratio between the difference (luminance variation range) and the maximum value is employed to characterize the image luminance homogeneity level, described as:

$$r = \frac{v_{\max} - v_{\min}}{v_{\max} + c} \quad (2)$$

where v_{\max} and v_{\min} represent the maximum value and the minimum value, respectively. c is a small constant to avoid instability, which is 0.0001. The greater the r value is, the lower the luminance homogeneity degree.

2) *Color Cast Evaluation*: Light of different wavelengths has different underwater attenuation rates, which easily leads to color casting in the acquired underwater images. Compared with green and blue light, red light has a greater attenuation rate and thus attenuates the most underwater. Therefore, underwater images often appear greenish or bluish. As noted in [51], for color cast underwater images, the chromaticity distribution on the ab chromaticity coordinate plane in CIELab color space tends to be a single peak or more concentrated (small variance), while the average value of the chromaticity tends to be large. In contrast, if the chromaticity distribution exhibits multiple peaks or is more dispersed (large variance) while the average value of the chromaticity is relatively small, the color cast degree of the underwater image decreases greatly.

The above observations offer an effective method for measuring the color cast degree of underwater images. Specifically, we first transform the underwater image I from RGB color space to CIELab color space. The average value of the chromaticity can be calculated as:

$$m_a = \frac{1}{N} \sum_{i=1}^N a(i), \quad m_b = \frac{1}{N} \sum_{i=1}^N b(i) \quad (3)$$

where m_a and m_b represent the average values of chrominance channels a and b, respectively. N refers to the pixel number of the image. Then, the average chrominance value can be defined by integrating m_a and m_b as:

$$m = \sqrt{m_a^2 + m_b^2} \quad (4)$$

Next, we calculate the variance values of channels a and b as follows:

$$v_a = \frac{1}{N} \sum_{i=1}^N [a(i) - m_a]^2, \quad v_b = \frac{1}{N} \sum_{i=1}^N [b(i) - m_b]^2 \quad (5)$$

where v_a and v_b represent the variance values of channels a and b, respectively. Similarly, the average variance value of the chrominance can be calculated as:

$$v = \sqrt{v_a^2 + v_b^2} \quad (6)$$

Then, the degree of the color cast can be evaluated by:

$$d = \frac{m}{v + \varepsilon} \quad (7)$$

where ε is a small constant to avoid instability, which takes 0.0001 empirically. The larger the d value is, the more serious the color cast of the underwater image.

To visually indicate the effectiveness of the color cast measure in characterizing the color cast degree of the underwater image, we select three underwater images of different color cast degrees and compute their color cast measures, i.e., d values, respectively, as shown in Fig. 3, where (a), (b) and (c) are slight, moderate and severe color cast images. The underwater image

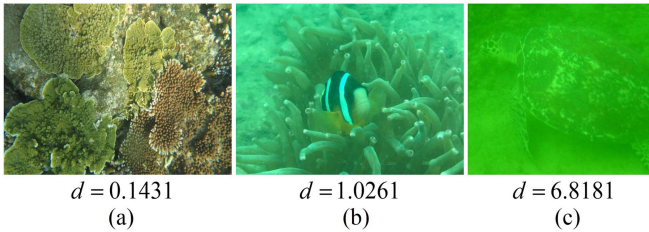


Fig. 3. Three underwater images of different degrees of color cast with their color cast measures. (a) slight color-cast image; (b) moderate color-cast image; (c) severe color-cast image. It is observed that the color cast measure d is consistent with the color cast degree of the image.

with a higher color cast degree has a greater d value, which indicates the efficacy of d for color cast measurement.

3) *Sharpness Evaluation*: Forward scattering, in which the light from the object deviates from its original direction before reaching the camera, causes blurring of the acquired underwater image [1]. Therefore, sharpness evaluation plays an essential role in the quality evaluation of underwater images. To estimate the sharpness degree of the underwater image, we employ a simple yet effective approach, which is the enhancement measure estimation (EME) method [52]. Specifically, we first apply the Sobel detector on each RGB channel of the image to extract the corresponding edge map. Then, we multiply each color channel with its edge map to obtain the grayscale edge map, denoted by E . The EME measure on each channel is subsequently computed as:

$$EME = \frac{2}{x \times y} \sum_{i=1}^x \sum_{j=1}^y \log \left(\frac{E_{\max,i,j}}{E_{\min,i,j}} \right) \quad (8)$$

where the underwater image is divided into xy blocks and $E_{\max,i,j}$ and $E_{\min,i,j}$ represent the maximum value and minimum value within the (i, j) block of the grayscale edge map, respectively. The sharpness level of the underwater image is estimated by integrating the EME measure on each color channel of the image, described as:

$$s = \lambda_R EME_R + \lambda_G EME_G + \lambda_B EME_B \quad (9)$$

where s indicates the image sharpness level and λ_R , λ_G and λ_B are parameters for integration, which are set to 0.299, 0.587 and 0.114, respectively, as suggested in [9].

4) *Contrast Evaluation*: The contrast of the underwater image can be affected by some factors, such as the limitation of the photographing device and undesirable photographing conditions [53]. It is well known that contrast has a significant impact on image quality. In this article, we characterize the image contrast from local and global perspectives. Specifically, we compute the contrast energy (CE) to evaluate the image local contrast, which evaluates the local contrast precisely and can be efficiently computed [54]. More specifically, CE is calculated on each color channel of the image, described as:

$$CE_{I_c} = \frac{\gamma \times G(I_c)}{G(I_c) + \gamma \times \tau} - n_c \quad (10)$$

where c refers to one color channel in $\{gray, yb, rg\}$. The $gray$ channel is obtained by $gray = 0.299R + 0.587G + 0.114B$,

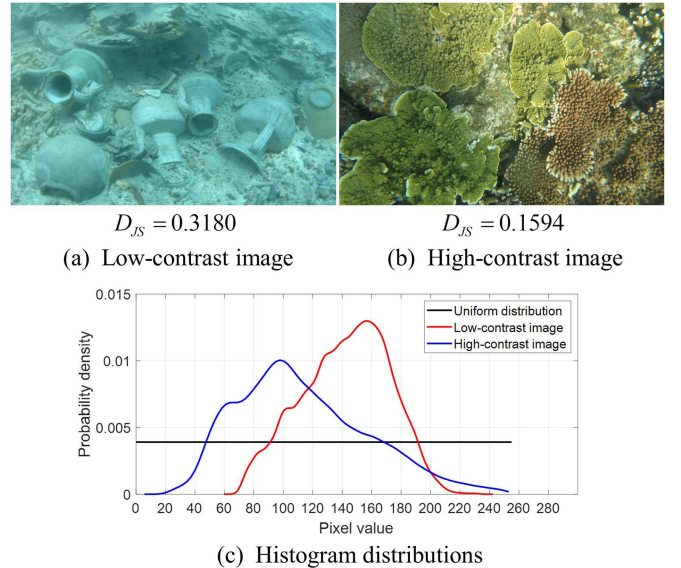


Fig. 4. High-contrast, Low-contrast underwater images with their gray-level histogram distributions and the corresponding D_{JS} values.

and the yb and rg channels are computed as $yb = 0.5(R + G) - B$, $rg = R - G$. $G(I_c) = \sqrt{(I_c \otimes g_h)^2 + (I_c \otimes g_v)^2}$, g_h and g_v stand for the horizontal and vertical second-order derivatives of the Gaussian function, and \otimes refers to the convolution operation. γ is the maximum value of $G(I_c)$, τ is the contrast gain parameter and n_c represents the noise threshold of color channel c . Through (10), we obtain three CE maps of the underwater image. Then, we pool the CE maps with their mean values and employ them to characterize the image local contrast level.

In contrast, we evaluate the global contrast of the underwater image by analyzing its gray-level histogram. In image processing, the gray-level histogram that depicts the pixel-value distribution can intuitively reflect the image contrast. Specifically, the histogram of a high-contrast image is usually relatively flat and covers a wide range in the pixel-value axis. In contrast, the histogram of a low-contrast image tends to concentrate and span a narrow range. We illustrate such regularity in Fig. 4, where we show one low-contrast underwater image and one high-contrast image and plot their gray-level histogram distributions. For convenient comparison, we also plot the uniform distribution as the baseline. It is clearly observed that the high-contrast underwater image has a flatter and wider distribution (depicted by the blue line in Fig. 4(c)), which is closer to the uniform distribution. However, the histogram distribution of the low-contrast image (depicted by the red line in Fig. 4(c)) is narrower and more concentrated. Therefore, the flatness level of the image gray-level histogram is a good indicator of the image global contrast. To characterize the flatness level, we can compute the divergence between the image histogram distribution and the uniform distribution. The smaller the divergence is, the higher the flatness level of the histogram. To this end, the popular Kullback-Leibler divergence (K-L divergence) that measures the distance between two probability distributions is employed to measure the discrepancy between the underwater image gray-level histogram

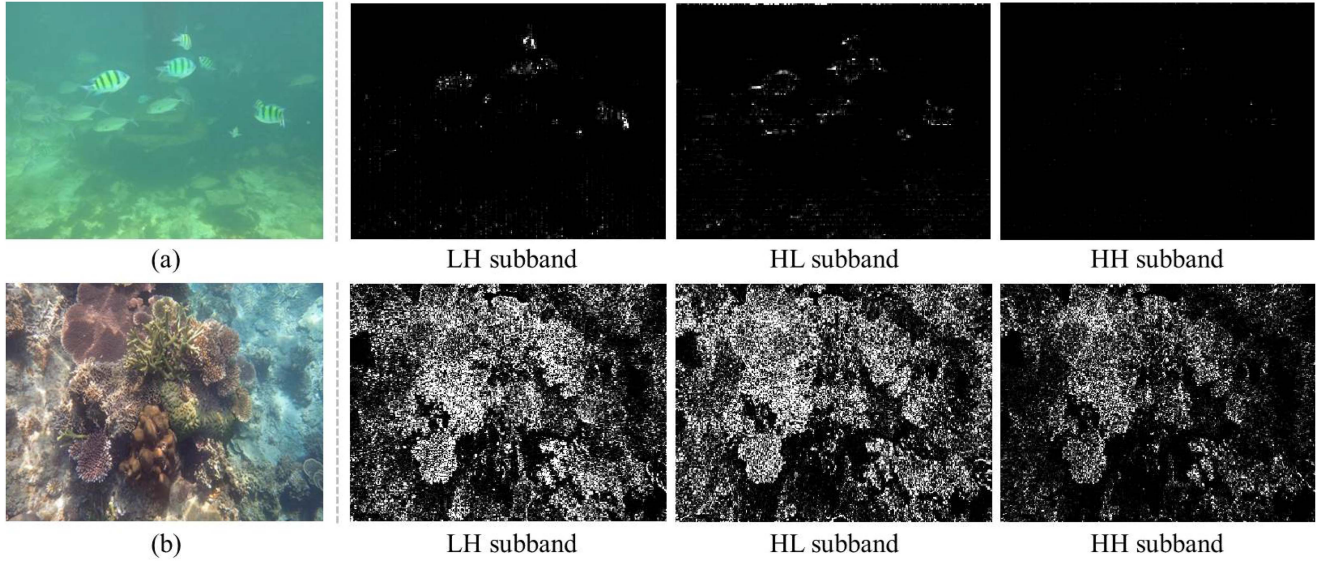


Fig. 5. Example underwater images of heavy and slight fog with their decomposed wavelet subbands, i.e., the LH, HL and HH-subbands. (a) heavy-fog underwater image; (b) slight-fog underwater image. It's clear to observe that the heavy-fog image contains much fewer details than the slight-fog image, as revealed by their wavelet subbands.

distribution and the uniform distribution. Specifically, assume \mathbf{p} and \mathbf{q} are the underwater image histogram distribution and the uniform distribution, respectively. The K-L divergence between \mathbf{p} and \mathbf{q} is defined as:

$$D_{KL}(\mathbf{p} \parallel \mathbf{q}) = - \int p(t) \log q(t) dt + \int p(t) \log p(t) dt \quad (11)$$

However, the K-L divergence measure is nonsymmetrical, namely, $D_{KL}(\mathbf{p} \parallel \mathbf{q}) \neq D_{KL}(\mathbf{q} \parallel \mathbf{p})$. Therefore, we employ the symmetrical Jensen-Shannon (J-S) divergence to improve the system stability, which is derived directly from the K-L divergence as:

$$D_{JS}(\mathbf{p} \parallel \mathbf{q}) = \frac{D_{KL}(\mathbf{p} \parallel \mathbf{v}) + D_{KL}(\mathbf{q} \parallel \mathbf{v})}{2} \quad (12)$$

where $\mathbf{v} = (\mathbf{p} + \mathbf{q})/2$. We take $D_{JS}(\mathbf{p} \parallel \mathbf{q})$ as the quality-aware feature to characterize the global contrast of the underwater image. In Fig. 4, we also compute the D_{JS} values of the high-contrast and low-contrast underwater images, shown below (a) and (b). One can see that the D_{JS} value of the low-contrast image is larger than that of the high-contrast image, as expected, which reveals the effectiveness of the D_{JS} value in characterizing the image contrast.

5) *Fog Density Evaluation*: Backward scattering (the light reflected by the water toward the camera before arriving at the object) generates unique fog and superimposes it on the underwater image [1], [10], which is a very common phenomenon in underwater images. The unique fog in underwater images will reduce image visibility and affect its quality accordingly. Therefore, characterizing the fog density or invisibility of underwater images is indispensable for underwater image quality evaluation. Similar to contrast evaluation, we characterize the fog density of the underwater image from local and global aspects.

On the one hand, as the fog superimposed on the image hides the image details, the heavier the fog density is, the fewer details the image contains. Therefore, characterizing the image detail is an effective strategy for evaluating the image fog density. In this article, we use the wavelet transform to extract the image details, which can be revealed by the high-frequency components in the wavelet subbands. To illustrate this visually, we choose two underwater images of different fog densities and decompose them into three-level wavelet subbands by applying the Cohen-Daubechies-Fauraue 9/7 filters [55]. The subbands of each level are composed of LH, HL and HH subbands. We show the two underwater images and their decomposed first-level subbands in Fig. 5, where (a) is the heavy-fog image, (b) is the slight-fog image, and the three wavelet subbands are on their right. In this figure, we can observe that the wavelet subbands can represent the local details in the image well. In addition, by comparing the subbands of the heavy-fog and slight-fog images, we find that most values of the subbands of the heavy-fog image are obviously smaller or tend to be zero, which demonstrates the feasibility of wavelet subbands in characterizing the fog density of the underwater image. To measure the image local fog density, we take the mean absolute value of the wavelet subbands. In the implementation, we calculate the logarithm of the result for suppressing large values, described as:

$$E_Z^k = \log_{10} \left(\frac{1}{N} \sum_{i,j} |Z_k(i,j)| + c \right) \quad (13)$$

where Z represents the LH, HL or HH subband and k refers to the wavelet subband level number, i.e., $k \in \{1, 2, 3\}$. N counts the number of values in each subband. c is a constant to guarantee that the result is nonnegative, which is set to 1. Then, we calculate the mean of the E value of each level to characterize the image

local fog density:

$$E_T = \frac{1}{3} \sum_{k=1}^3 \frac{E_{LH}^k + E_{HL}^k + 2\gamma E_{HH}^k}{2(1+\gamma)} \quad (14)$$

where γ is a parameter to adjust the importance of different subbands. We set γ to 4.

On the other hand, we characterize the global fog density of the image for quality evaluation. As indicated in [54], the distribution of the locally mean subtracted and contrast normalized (MSCN) coefficients of the image is very sensitive to the image global fog density. Specifically, according to [22], the MSCN coefficients of an image I are defined by:

$$C(i, j) = \frac{I(i, j) - \mu(i, j)}{\sigma(i, j) + 1} \quad (15)$$

where (i, j) denotes the pixel coordinate and $C(i, j)$ refers to the MSCN coefficient at (i, j) . $\mu(i, j)$ and $\sigma(i, j)$ are the mean and standard deviation, respectively:

$$\mu(i, j) = \sum_{u=-U}^U \sum_{v=-V}^V g_{u,v} I(i+u, j+v) \quad (16)$$

$$\sigma(i, j) = \sqrt{\sum_{u=-U}^U \sum_{v=-V}^V g_{u,v} [I(i+u, j+v) - \mu(i, j)]^2} \quad (17)$$

where $g = \{g_{u,v} \mid u = -U, \dots, U; v = -V, \dots, V\}$ represents a 2D circularly symmetric Gaussian weighting filter. Then, the distribution of MSCN coefficients is well fitted with the zero-mean generalized Gaussian distribution (GGD) model, defined as:

$$G(x; \lambda, k) = \frac{\lambda}{2k\Gamma(1/\lambda)} \exp\left(-\left(\frac{|x|}{k}\right)^\lambda\right) \quad (18)$$

where λ and k represent the GGD model parameters. $\Gamma(\cdot)$ is the gamma function, defined as:

$$\Gamma(t) = \int_0^\infty \phi^{t-1} e^{-\phi} d\phi, \quad t > 0 \quad (19)$$

The moment matching-based approach [56] is employed to obtain λ and k , which serve as the quality-aware features to characterize the global fog density of the underwater image.

6) *Noiseness Evaluation*: In UIQI, we finally examine the noise level in the underwater image. Many methods have been proposed to characterize the image noise level. For instance, Zhai et al. exploited natural scene statistics for noise estimation [57]. Zoran et al. took advantage of the scale invariant statistics property to characterize image noise [58]. Although these methods can evaluate image noise with high accuracy, they also involve complex image transformation or optimization problem solving, which has a high computational cost. In this article, we devise much more efficient approaches to characterize the image noise level. As indicated in [59], images of various noise levels respond differently when going through a fixed low-pass filter. More specifically, the spatial frequency of an image with a higher noise level degenerates more than that of an image with less noise after low-pass filtering. Accordingly, the divergence

TABLE I
SUMMARY OF THE QUALITY-AWARE FEATURES IN UIQI

Index	Feature type	Dimension
1	Luminance	2
2	Color cast	1
3	Sharpness	1
4	Contrast	4
5	Fog density	3
6	Noiseness	3

between an underwater image with a higher noise level and its corresponding low-pass filtered version should be larger than that of an underwater image with a lower noise level. To illustrate this fact, we select three underwater images of different noise levels. Then, we calculate the differences between them and their low-pass filtered images pixel-by-pixel, denoted as:

$$D = I - \mathbb{G}(I) \quad (20)$$

where I refers to the input underwater image and $\mathbb{G}(\cdot)$ refers to the Gaussian low-pass filtering function. The three images and the difference distributions are clearly shown in Fig. 6, where (a)(b)(c) are the slight-noise, moderate-noise and heavy-noise images, respectively, and (d) illustrates their difference distributions. As the noise level increases, the difference distribution becomes flatter and wider, which means that more difference values deviate from 0. These observations verify that more spatial frequency decays in the image of a higher noise level. Moreover, we can see that the difference distribution can be nicely fitted with the zero-mean GGD model. Therefore, we fit the difference distribution with (18) and (19) and then employ the model parameters to characterize the image noise degree. In addition, the entropy value that characterizes the information amount of a variable is very powerful for measuring the quality degradation degrees [5], [60]; hence, we also calculate the entropy of the difference D and introduce it into our quality-aware features to characterize the image noise level, which is computed as:

$$e = - \sum_i p_i \log_2 p_i \quad (21)$$

where p_i refers to the probability that the value of D equals i .

We have designed dedicated features to measure the image luminance, color cast, sharpness, contrast, fog density and noise to comprehensively characterize underwater image quality. For convenient reading, we summarize the extracted features in Table I clearly. It is easy to find that the total dimension of the features in the UIQI for quality evaluation is 14. All the quality-aware features are concatenated into a feature vector, which is used to characterize the underwater image quality.

B. Quality Evaluation of the Underwater Image

To evaluate the underwater image quality with the extracted quality-aware features, a regression model that maps the features to the image quality score is needed. Here, we employ the support vector regression (SVR) technique to implement this goal, which has good generalization capability

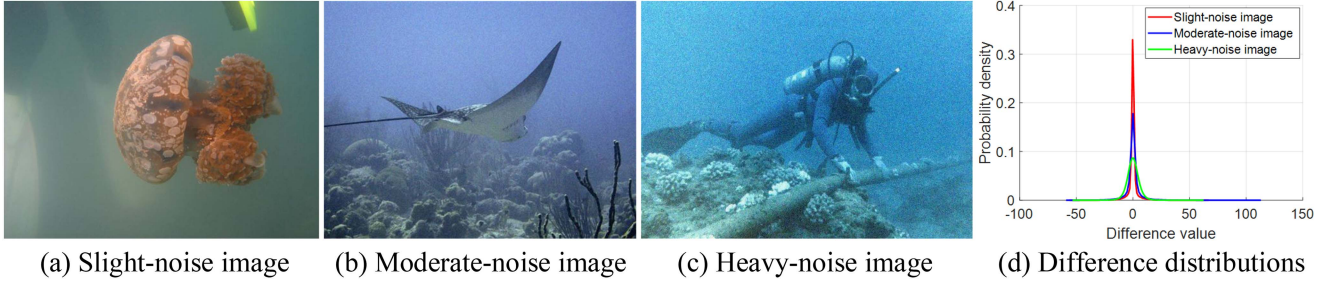


Fig. 6. Underwater image of different noisiness levels and their difference distributions. (a) Slight-noise underwater image; (b) Moderate-noise underwater image; (c) Heavy-noise underwater image; (d) Difference distributions of the three underwater images.



Fig. 7. Example underwater images in UWIQA database [11].

and has been pervasively adopted in many successful NR IQA works [22], [61], [62]. Specifically, given a training set $\{(\mathbf{x}_1, s_1), (\mathbf{x}_2, s_2), \dots, (\mathbf{x}_k, s_k)\}$, where \mathbf{x}_i , $i = 1, 2, \dots, k$ represents the quality-aware feature vector and s_i represents the corresponding MOS value. We aim to find a function f that predicts the underwater image quality score, denoted as:

$$f(\mathbf{x}) = \mathbf{w}^T \phi(\mathbf{x}) + b \quad (22)$$

where $\phi(\cdot)$ maps the quality-aware feature vector \mathbf{x} from low dimension to high dimension, \mathbf{w} and b are the model parameters, which can be obtained by solving the following optimization problem:

$$\begin{aligned} & \min \frac{1}{2} \|\mathbf{w}\|^2 + \eta \left(\sum_{i=1}^k \xi_i + \sum_{i=1}^k \hat{\xi}_i \right) \\ & \text{s.t. } f(\mathbf{x}_i) - s_i \leq \varepsilon + \xi_i \\ & \quad s_i - f(\mathbf{x}_i) \leq \varepsilon + \hat{\xi}_i \\ & \quad \xi_i, \hat{\xi}_i \geq 0, i = 1, 2, \dots, k \end{aligned} \quad (23)$$

where ξ_i and $\hat{\xi}_i$ are two slack variables and η is a constant to adjust the importance of the two terms. In this article, we exploit the LIBSVM package [63] with the radial basis function (RBF) kernel to implement SVR. After obtaining \mathbf{w} and b , we use them to predict the quality score of a new given underwater image.

IV. EXPERIMENTAL RESULTS AND ANALYSIS

A. Testing Image Database

To test the prediction performance of our proposed UIQI model, we perform experiments on a large-scale underwater

image quality assessment (UWIQA) [11], which contains a total of 890 underwater images taken from the underwater image database [66]. Here, we present some example images in Fig. 7. It is clearly observed that the underwater images in UWIQA cover a wide variety of typical underwater scenes, such as fish, rock, coral, plants, and artificial facilities. In the meantime, underwater images have typical degenerate types, such as color cast, blur, low contrast, noise, and fog. Twenty-one observers, composed of 11 males and 10 females, participated in the subjective quality annotations of the underwater images. In summary, UWIQA is quite suitable for testing underwater IQA methods. More details about the UWIQA database can be found in [11].

B. Experimental Protocol

To quantify the prediction performance of the underwater IQA models, we employ four popular statistical indices: the Spearman rank order correlation coefficient (SRCC), Kendalls rank correlation coefficient (KRCC), Pearsons linear correlation coefficient (PLCC) and root mean square error (RMSE) [67]. These four indices are computed between the objective scores delivered by the IQA methods and the subjective MOS values. A superior IQA model is able to achieve higher absolute values of SRCC, KRCC and PLCC but lower values of RMSE. As suggested by the video quality experts group (VQEG) [67], before computing the above four statistical measures, the objective scores of the IQA methods should be mapped onto the subjective MOS values via a five-parameter logistic function, defined as:

$$m(q) = \theta_1 \left(\frac{1}{2} - \frac{1}{1 + \exp(\theta_2 \cdot (q - \theta_3))} \right) + \theta_4 \cdot q + \theta_5 \quad (24)$$

TABLE II
PREDICTION PERFORMANCE MEASURED BY SRCC, KRCC, PLCC AND RMSE ON THE UWIQA DATABASE. THE TOP THREE PERFORMANCE VALUES IN EACH COLUMN ARE HIGHLIGHTED WITH BOLDFACE

IQA Method	SRCC	KRCC	PLCC	RMSE
BRISQUE [22]	0.3456	0.2562	0.3669	0.1415
NFERM [64]	0.3486	0.2595	0.3925	0.1398
NIQE [25]	0.4347	0.3243	0.4687	0.1343
IL-NIQE [26]	0.4686	0.3476	0.4421	0.1364
SNP-NIQE [7]	0.5516	0.4199	0.5897	0.1228
PIQE [65]	0.2084	0.1492	0.3224	0.1441
NPQI [60]	0.6078	0.4667	0.6361	0.1173
dipIQ [33]	0.0869	0.0641	0.1369	0.1506
HyperIQA [36]	0.6501	0.5040	0.6799	0.1114
UNIQUE [37]	0.2496	0.1835	0.2386	0.1476
UCIQE [1]	0.6271	0.4863	0.6261	0.1185
UIQM [9]	0.5960	0.4563	0.5928	0.1225
CCF [10]	0.4456	0.3344	0.4634	0.1348
FDUM [11]	0.6780	0.5289	0.6462	0.1160
URQ [41]	0.3724	0.2737	0.3527	0.1423
UIQI (Pro.)	0.7423	0.5912	0.7412	0.1020

where $m(q)$ refers to the mapped quality score, q refers to the objective quality score of the IQA models, and $\theta_1 \sim \theta_5$ refers to the model parameters.

Since the underwater images in UWIQA lack the corresponding original pristine images, FR and RR IQA models cannot be applied. Therefore, we compare our proposed UIQI with representative NR IQA methods, which include BRISQUE [22], NFERM [64], NIQE [25], IL-NIQE [26], SNP-NIQE [7], PIQE [65], NPQI [60], dipIQ [33], HyperIQA [36], UNIQUE [37], UCIQE [1], UIQM [9], CCF [10], FDUM [11], and URQ [41]. Among them, BRISQUE, NFERM, NIQE, IL-NIQE, SNP-NIQE, PIQE, NPQI, dipIQ, HyperIQA, and UNIQUE are the NR IQA approaches for natural images, and UCIQE, UIQM, CCF, FDUM and URQ are the specialized underwater IQA models.

C. Quality Prediction Performance Comparison

As the proposed UIQI needs to train a regression module for quality prediction, we follow the widely used train-test strategy in NR IQA works, which randomly divides the image database (UWIQA) into two parts, one containing 80% images for training the quality prediction module and the other containing the remaining 20% images for testing the quality model [22], [53], [64]. To eliminate performance bias and demonstrate that the proposed quality model is not decided by a specific train-test split, we repeat this random 80% train-20% test process 1,000 times. The mean performance measured by SRCC, KRCC, PLCC and RMSE of the 1,000-time experiments on the testing dataset is listed in Table II, where the top three performance values in each column are highlighted with boldface.

In Table II, we observe that the NR IQA models for natural images, e.g., NPQI and HyperIQA, have a certain ability to

evaluate underwater image quality due to their general applicability for evaluating image quality. However, most models that perform well on natural images still cannot yield desirable performance on underwater images, such as PIQE and dipIQ. These observations manifest that underwater images do have different degradation characteristics from natural images. Among them, HyperIQA and NPQI achieve relatively high prediction accuracy, as HyperIQA deeply investigates content understanding (image semantics) and integrates it into IQA, while NPQI deeply investigates the perceptual characteristics of the human brain for IQA, which both have strong general applicability for natural and underwater IQA. Compared with the natural image IQA methods, it is not surprising to find that most underwater IQA methods can achieve better prediction performance. It is worth noting that the proposed UIQI performs best and outperforms other competitors by a large margin, which strongly verifies the rationality of analyzing more image properties for underwater IQA and the effectiveness of the designed quality-aware features in UIQI in characterizing the underwater image quality. By comparison, other underwater IQA models that characterize limited image properties can only achieve moderate or even unsatisfying prediction accuracy.

To more intuitively demonstrate the consistency between the IQA methods and the subjective MOS values, we select eight underwater images of different subjective qualities from the UWIQA database and apply all IQA methods to compute their quality scores. The underwater images are shown in Fig. 8, and the corresponding objective quality scores predicted by the IQA methods are reported in Table III, in which the symbol “↑” behind each IQA method represents that the higher score delivered by this method indicates better image quality. In contrast, the symbol “↓” behind each method represents that the lower score of this method indicates better image quality. We also rank the image quality according to the objective quality scores of each IQA method and present the rank numbers in brackets.

By observing Table III, we can obtain some meaningful findings. First, existing IQA methods for natural images cannot deliver consistent quality results with subjective MOS values, and some methods even give completely opposite results. For example, Fig. 8(h) has the worst visual quality, whose MOS value equals 0.2. However, according to the PIQE method, this image quality ranks first and has the best image quality. Similarly, NFERM regards this image as having the second-best image quality. Fig. 8(g) has the second worst image quality, while dipIQ and UNIQUE regard it as having the best image quality. The competing underwater IQA methods cannot distinguish the underwater image quality correctly as well. For example, UCIQE confuses the quality of Fig. 8(b) and (c) and the quality of Fig. 8(d) and (e). UIQM confuses the quality of Fig. 8(b) and (c), the quality of Fig. 8(d) and (e) and the quality of Fig. 8(g) and (h). Other underwater IQA competitors predict more wrong quality rankings. It is clear that the proposed UIQI can yield consistent quality rankings with the subjective MOS values, which demonstrates the favorable ability of the UIQI in distinguishing the underwater image quality.

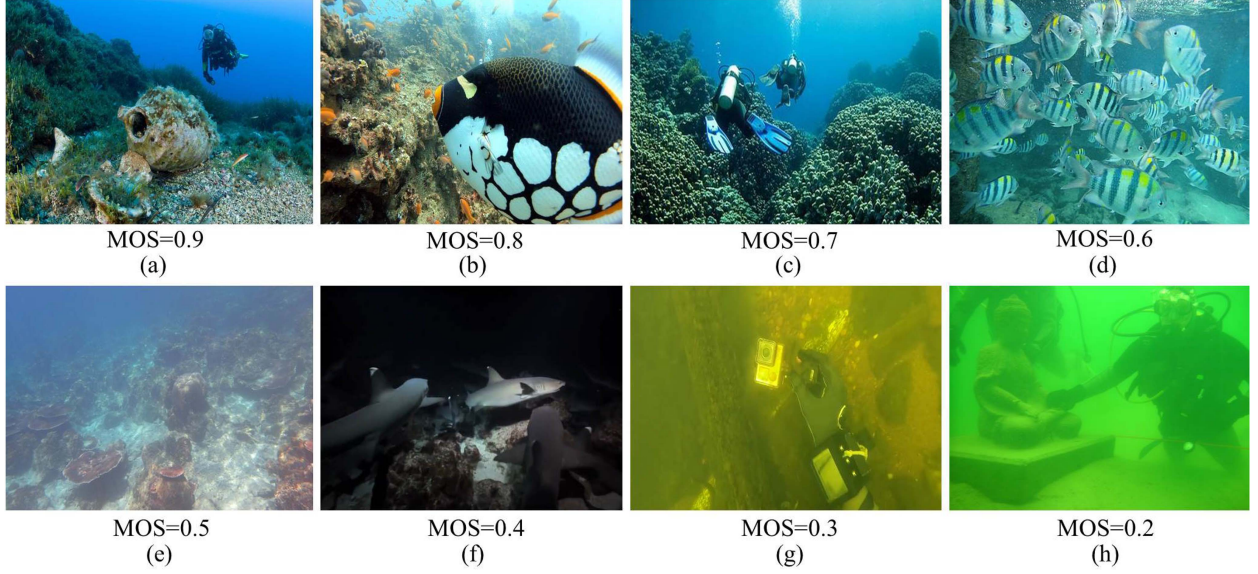


Fig. 8. Underwater images of different subjective quality. The higher MOS value indicates better image quality.

TABLE III
MOS VALUES AND OBJECTIVE QUALITY SCORES PREDICTED BY THE IQA METHODS OF THE UNDERWATER IMAGES IN FIG. 8. THE NUMBER IN THE BRACKETS REFERS TO THE QUALITY RANK NUMBER ACCORDING TO MOS OR EACH IQA METHOD

	Fig. 8 (a)	Fig. 8 (b)	Fig. 8 (c)	Fig. 8 (d)	Fig. 8 (e)	Fig. 8 (f)	Fig. 8 (g)	Fig. 8 (h)
MOS (Ground truth)	0.9 (1)	0.8 (2)	0.7 (3)	0.6 (4)	0.5 (5)	0.4 (6)	0.3 (7)	0.2 (8)
BRISQUE [22] (\uparrow)	0.6386 (1)	0.6243 (2)	0.4974 (8)	0.5007 (7)	0.5383 (4)	0.5124 (5)	0.5889 (3)	0.5021 (6)
NFERM [64] (\uparrow)	0.6883 (3)	0.6928 (1)	0.5095 (6)	0.5286 (4)	0.4796 (7)	0.5110 (5)	0.3685 (8)	0.6897 (2)
NIQE [25] (\downarrow)	2.1141 (1)	2.6852 (2)	6.8129 (4)	3.4929 (3)	18.5586 (8)	7.1692 (6)	7.0939 (5)	8.3398 (7)
IL-NIQE [26] (\downarrow)	23.8519 (3)	17.3602 (1)	41.3451 (6)	18.3372 (2)	58.1182 (8)	33.2063 (4)	34.8289 (5)	55.8821 (7)
SNP-NIQE [7] (\downarrow)	3.3420 (1)	4.0462 (2)	7.4101 (4)	6.9708 (3)	22.8925 (8)	11.7738 (6)	9.7729 (5)	12.5333 (7)
PIQE [65] (\downarrow)	31.7844 (2)	34.4559 (4)	39.1861 (5)	32.8466 (3)	46.0535 (6)	64.5098 (8)	54.8411 (7)	7.0233 (1)
NPQI [60] (\downarrow)	3.7873 (1)	4.3539 (2)	9.1585 (4)	8.1506 (3)	102.7363 (8)	15.8425 (6)	12.0952 (5)	19.8938 (7)
dipIQ [33] (\uparrow)	-7.0445 (5)	-3.7943 (4)	-2.1332 (2)	-9.3835 (7)	-2.3022 (3)	-7.3323 (6)	-1.8703 (1)	-9.8172 (8)
HyperIQA [36] (\uparrow)	0.6487 (2)	0.6605 (1)	0.5209 (5)	0.5551 (3)	0.3939 (7)	0.4559 (6)	0.5309 (4)	0.3667 (8)
UNIQUE [37] (\uparrow)	0.8216 (2)	0.8000 (4)	0.6714 (7)	0.6197 (8)	0.7219 (5)	0.8141 (3)	0.9512 (1)	0.6983 (6)
UCIQE [1] (\uparrow)	35.8752 (1)	32.2376 (3)	32.7884 (2)	30.6955 (5)	31.9299 (4)	27.0893 (6)	26.3908 (7)	19.0256 (8)
UIQM [9] (\uparrow)	1.7310 (1)	1.5228 (3)	1.6125 (2)	1.2535 (5)	1.4972 (4)	1.1841 (6)	0.5913 (8)	0.6035 (7)
CCF [10] (\uparrow)	26.9893 (4)	34.8443 (2)	37.9844 (1)	23.7656 (5)	31.2540 (3)	14.1339 (7)	21.6344 (6)	8.1107 (8)
FDUM [11] (\uparrow)	1.0136 (2)	0.7822 (3)	1.1714 (1)	0.4152 (5)	0.7635 (4)	0.1921 (7)	0.2699 (6)	0.1176 (8)
URQ [41] (\uparrow)	0.7558 (4)	0.8527 (1)	0.7636 (3)	0.7845 (2)	0.7107 (5)	0.4821 (8)	0.6014 (6)	0.6003 (7)
UIQI (Pro.) (\uparrow)	0.7923 (1)	0.7069 (2)	0.6023 (3)	0.5600 (4)	0.5368 (5)	0.4282 (6)	0.4198 (7)	0.2325 (8)

D. Prediction Performance Evaluation of Other Train-Test Partitions

In addition to the 80% train-20% test methodology, we also tested other train-test ratios of the UIQI. Specifically, we randomly select 10%, 20%, 30%, 40%, 50%, 60%, 70%, 80% and 90% images of the UWIQA database for training the quality prediction model. Correspondingly, the remaining 90%, 80%, 70%, 60%, 50%, 40%, 30%, 20% and 10% images are used for testing the quality model. We repeated each train-test experiment 1,000 times and showed the mean prediction performance on the testing set in Fig. 9, where SRCC is employed as the performance measure. From this figure, we observe that the prediction performance remains relatively stable among different proportions of training data. As the training data proportion decreases, the

prediction performance decreases slightly. A high-performance quality model can be obtained by training on 10% of UWIQA images. These observations can be attributed to the fact that the quality-aware features in the UIQI can capture the essential image properties in evaluating the underwater image quality. Therefore, different train-test ratios have little effect on the UIQI prediction performance.

E. Statistical Significance Test

To examine the statistical significance of the IQA metrics, we applied a t test on the prediction residuals between the subjective MOS values and the objective quality scores predicted by the IQA methods on the UWIQA database. The experimental results are reported in Table IV. A t test result of -1, 0 or 1 implies that

TABLE IV
T-TEST RESULTS OF IQA METHODS ON THE UWIQA DATABASE. –1, 0 OR 1 OF T-TEST IMPLIES THAT THE PROPOSED UIQI IS INFERIOR, EQUAL OR SUPERIOR TO THE OTHER IQA COMPETITORS STATISTICALLY (95% CONFIDENCE)

BRISQUE	NFERM	NIQE	IL-NIQE	SNP-NIQE	PIQE	NPQI	dipIQ	HyperIQA	UNIQUE	UCIQE	UIQM	CCF	FDUM	URQ
1	1	1	1	1	1	1	1	1	1	1	1	1	1	1

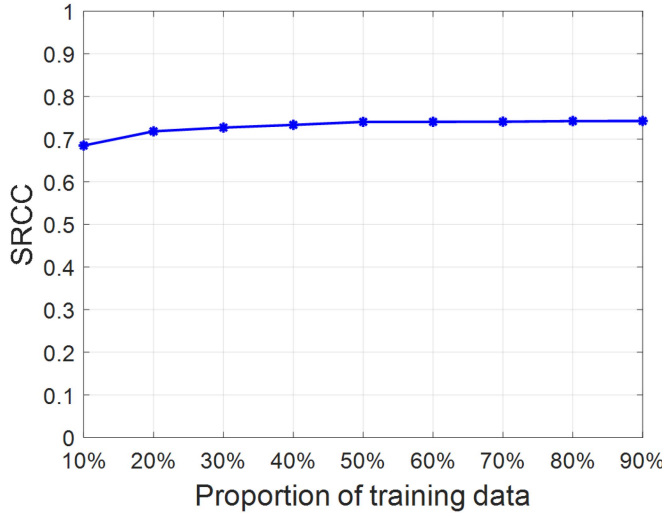


Fig. 9. Prediction performance measured by SRCC of different proportions of data for training.

the proposed UIQI is inferior, equal, or superior to other IQA methods statistically (95% confidence). In Table IV, we observe that the test results are all 1, which verifies that the proposed UIQI is statistically better than all the other IQA methods.

F. Cross-Database Validation

Generalization capability is quite important for the practical application of an IQA method. Therefore, to further evaluate the generalization capability of the proposed UIQI, we trained the prediction model on the entire UWIQA database and tested it on a new underwater image quality dataset, which was constructed in [10]. Specifically, the new underwater image database contains 87 underwater images, which were acquired by photographing a colorchecker in a water tank. The underwater images can be classified into ten groups according to different capture distances and water turbidity. Twenty graduate students participated in the subjective quality annotations of the underwater images. More details about this new underwater image quality database can be found in [10]. The prediction performance on the new underwater image database measured by SRCC, KRCC, PLCC and RMSE are reported in Table V, where the top three performance values in each column are highlighted with boldface.

In Table V, it can be found that most of the IQA methods for natural images cannot deliver desirable prediction performance on the new underwater image database. The best performer NPQI only achieves moderate prediction accuracy. Most of the specialized underwater IQA methods perform better than the IQA methods for natural images, as expected. The proposed UIQI achieves the best prediction performance, which is

TABLE V
CROSS-DATABASE VALIDATION RESULTS MEASURED BY SRCC, KRCC, PLCC AND RMSE ON THE NEW UNDERWATER IMAGE DATABASE [10]. THE TOP THREE PERFORMANCE VALUES IN EACH COLUMN ARE HIGHLIGHTED WITH BOLDFACE

IQA Method	SRCC	KRCC	PLCC	RMSE
BRISQUE [22]	0.1473	0.1082	0.3176	25.3556
NFERM [64]	0.5471	0.3899	0.5947	21.4967
NIQE [25]	0.2266	0.1633	0.3430	25.1181
IL-NIQE [26]	0.6437	0.4766	0.7121	18.7745
SNP-NIQE [7]	0.4475	0.3315	0.5392	22.5200
PIQE [65]	0.0268	0.0230	0.1318	26.5068
NPQI [60]	0.7076	0.5409	0.7357	18.1116
dipIQ [33]	0.2685	0.1917	0.3051	25.4649
HyperIQA [36]	0.4324	0.2968	0.4819	23.4313
UNIQUE [37]	0.0743	0.0445	0.0706	26.6733
UCIQE [1]	0.7394	0.5757	0.7550	17.5344
UIQM [9]	0.4118	0.3154	0.4858	23.3721
CCF [10]	0.8006	0.6384	0.8671	13.3218
FDUM [11]	0.8753	0.7171	0.9168	10.6760
URQ [41]	0.9193	0.7487	0.9193	10.5219
UIQI (Pro.)	0.9004	0.7366	0.9320	9.3484

comparable to that of URQ, indicating that the quality-aware features in the UIQI can characterize the essential properties of the underwater image so that the UIQI can generalize well to new underwater images. By comparing Table II, we also find that the UIQI prediction performance on the new underwater image database is much higher than that on the UWIQA database. These observations can be attributed to the divergent characteristics of these two databases. Specifically, the images in UWIQA involve rich underwater scenes and complicated quality degradation conditions. However, by observing the images in the new underwater image database, we find that all images involve simple underwater scenes (a color checker), and more importantly, the degradation conditions are much simpler, i.e., all the images mainly suffer from insufficient luminance. Therefore, for the complicated UWIQA database, there inevitably exist more factors affecting the underwater image quality that we have not considered in the UIQI, which raises greater challenges for the UIQI to evaluate the image quality. For the simple new underwater image database, as the underwater image luminance is effectively characterized by the UIQI, which plays the leading role in affecting the image quality, the UIQI can deliver much better prediction performance on the new database.

G. Prediction Performance Evaluation of Each Type of Feature in the UIQI

In the UIQI, we designed six types of features to characterize the luminance, sharpness, color cast, contrast, fog and noise in

TABLE VI
PREDICTION PERFORMANCE OF REMOVING EACH TYPE OF FEATURES IN UIQI
ON THE UWIQA DATABASE

Removed Features	SRCC	KRCC	PLCC	RMSE
Luminance	0.7314	0.5798	0.7282	0.1042
Color cast	0.7224	0.5752	0.7245	0.1051
Sharpness	0.7021	0.5612	0.7117	0.1080
Contrast	0.6881	0.5391	0.6907	0.1100
Fog density	0.7133	0.5711	0.7201	0.1062
Noiseness	0.7190	0.5723	0.7220	0.1059
UIQI (Pro.)	0.7423	0.5912	0.7412	0.1020

the underwater image to comprehensively evaluate the image quality. It is necessary to be aware of the individual contribution of each type of feature to the overall prediction performance. To this end, we construct the quality prediction model by removing each type of feature and keeping the other types of features. The experimental procedure is consistent with that in subsection IV-C. Specifically, we performed 1000-time 80% train-20% test experiments on the UWIQA database. The mean performance in terms of SRCC, KRCC, PLCC and RMSE is reported in Table VI. For convenient comparison, we also list the prediction performance of the UIQI that contains all types of features.

By observing Table VI, it is not difficult to find that removing any single type of feature leads to performance degradation to some extent, which indicates that each type of feature in the UIQI can play a role in underwater image quality evaluation. Among all types of features, the contrast features contribute most to the overall prediction performance, as the performance of removing the contrast features is the lowest. Furthermore, the sharpness features are very important in characterizing the image quality, which can be verified by the observation that removing the sharpness features leads to significant performance degradation compared with the UIQI. It is interesting to find that features that characterize fog density and color cast are influential in quality evaluation, as the performance degradation is obvious when these two types of features are removed. This is because fog and color cast are very common phenomena in underwater images. In addition, we observe that removing the noise feature leads to noticeable performance degradation, which indicates that noise evaluation is indispensable in characterizing underwater image quality. By comparison, removing luminance features brings minimal performance loss, which implies that the contribution of luminance features is minimal among all types of features. Finally, the UIQI that contains all types of quality-aware features achieves the highest prediction accuracy, which indicates that different types of features in the UIQI that characterize different image properties can evaluate the image quality in a complementary manner.

H. Computational Time Evaluation

Finally, we evaluate the computational time of the IQA methods, which indicates the practicability of deploying IQA algorithms. Specifically, we chose three representative images in the UWIQA database whose resolutions are 640×480 , 1024×768

TABLE VII
COMPUTATIONAL TIME (MEASURED IN SECONDS) COMPARISON OF IQA
MODELS

IQA Method	640×480	1024×768	1920×1080
BRISQUE [22]	0.18	0.27	0.54
NFERM [64]	22.75	58.24	151.16
NIQE [25]	0.11	0.27	0.71
IL-NIQE [26]	3.19	3.39	3.83
SNP-NIQE [7]	1.82	5.10	20.68
PIQE [65]	0.07	0.16	0.39
NPQI [60]	1.57	3.96	9.70
dipIQ [33]	1.71	1.84	2.36
HyperIQA [36]	0.91	1.02	1.15
UNIQUE [37]	0.86	0.93	1.07
UCIQE [1]	0.10	0.26	0.73
UIQM [9]	0.17	0.53	1.17
CCF [10]	0.64	1.63	4.30
FDUM [11]	1.41	3.70	9.77
URQ [41]	0.05	0.14	0.37
UIQI (Pro.)	0.62	1.13	2.18

and 1920×1080 . We ran all the IQA methods on the three images and recorded their respective computational times, which were measured in seconds and tabulated in Table VII. The experiments were performed on a computer with a 3.0-GHz Intel Core i5-9500 CPU, 8 GB RAM and a graphics card NVIDIA 1080 Ti with 11 G graphics RAM. The software platforms were MATLAB R2019b and PyTorch. In Table VII, we observe that our proposed UIQI has a relatively moderate running speed. However, the computational time of UIQI has great potential to be further optimized, as different types of features in UIQI can be computed concurrently.

V. CONCLUSION

In this article, we evaluated the quality of underwater images and proposed a novel dedicated underwater IQA method named UIQI. Different from the existing underwater IQA approaches that characterize a small number of image properties for quality evaluation, in UIQI, six types of quality-aware features were carefully designed to characterize the image luminance, sharpness, color cast, contrast, fog density and noise, which describe the underwater image quality more comprehensively. After feature extraction, we employ SVR to integrate all the quality-aware features and predict the image quality score. Thorough tests performed on standard underwater image quality databases verify that the proposed UIQI achieves more promising prediction performance than the state-of-the-art NR IQA methods for both natural and underwater images.

REFERENCES

- [1] M. Yang and A. Sowmya, "An underwater color image quality evaluation metric," *IEEE Trans. Image Process.*, vol. 24, no. 12, pp. 6062–6071, Dec. 2015.
- [2] Z. Wang, A. C. Bovik, H. R. Sheikh, and E. P. Simoncelli, "Image quality assessment: From error visibility to structural similarity," *IEEE Trans. Image Process.*, vol. 13, no. 4, pp. 600–612, Apr. 2004.

- [3] L. Zhang, Y. Shen, and H. Li, "VSI: A visual saliency-induced index for perceptual image quality assessment," *IEEE Trans. Image Process.*, vol. 23, no. 10, pp. 4270–4281, Oct. 2014.
- [4] W. Xue, L. Zhang, X. Mou, and A. C. Bovik, "Gradient magnitude similarity deviation: A highly efficient perceptual image quality index," *IEEE Trans. Image Process.*, vol. 23, no. 2, pp. 684–695, Feb. 2014.
- [5] Y. Liu et al., "Reduced-reference image quality assessment in free-energy principle and sparse representation," *IEEE Trans. Multimedia*, vol. 20, no. 2, pp. 379–391, Feb. 2018.
- [6] G. Zhai, X. Wu, X. Yang, W. Lin, and W. Zhang, "A psychovisual quality metric in free-energy principle," *IEEE Trans. Image Process.*, vol. 21, no. 1, pp. 41–52, Jan. 2012.
- [7] Y. Liu et al., "Unsupervised blind image quality evaluation via statistical measurements of structure, naturalness, and perception," *IEEE Trans. Circuits Syst. Video Technol.*, vol. 30, no. 4, pp. 929–943, Apr. 2020.
- [8] Y. Liu et al., "Quality assessment for real out-of-focus blurred images," *J. Vis. Commun. Image Represent.*, vol. 46, pp. 70–80, 2017.
- [9] K. Panetta, C. Gao, and S. Agaian, "Human-visual-system-inspired underwater image quality measures," *IEEE J. Ocean. Eng.*, vol. 41, no. 3, pp. 541–551, Jul. 2016.
- [10] Y. Wang et al., "An imaging-inspired no-reference underwater color image quality assessment metric," *Comput. Electr. Eng.*, vol. 70, pp. 904–913, 2018.
- [11] N. Yang et al., "A reference-free underwater image quality assessment metric in frequency domain," *Signal Process., Image Commun.*, vol. 94, 2021, Art. no. 116218.
- [12] Z. Wang, E. Simoncelli, and A. Bovik, "Multiscale structural similarity for image quality assessment," in *Proc. IEEE Conf. Rec. 37th Asilomar Conf. Signals, Syst. Comput.*, 2003, pp. 1398–1402.
- [13] Z. Wang and Q. Li, "Information content weighting for perceptual image quality assessment," *IEEE Trans. Image Process.*, vol. 20, no. 5, pp. 1185–1198, May 2011.
- [14] K. Gu, G. Zhai, X. Yang, and W. Zhang, "An improved full-reference image quality metric based on structure compensation," in *Proc. Asia Pac. Signal Inf. Process. Assoc. ASC*, 2012, pp. 1–6.
- [15] H. R. Sheikh and A. C. Bovik, "Image information and visual quality," *IEEE Trans. Image Process.*, vol. 15, no. 2, pp. 430–444, Feb. 2006.
- [16] L. Zhang, L. Zhang, X. Mou, and D. Zhang, "FSIM: A feature similarity index for image quality assessment," *IEEE Trans. Image Process.*, vol. 20, no. 8, pp. 2378–2386, Aug. 2011.
- [17] K. Gu, L. Li, H. Lu, X. Min, and W. Lin, "A fast reliable image quality predictor by fusing micro-and macro-structures," *IEEE Trans. Ind. Electron.*, vol. 64, no. 5, pp. 3903–3912, May 2017.
- [18] R. Soundararajan and A. C. Bovik, "RRED indices: Reduced reference entropic differencing for image quality assessment," *IEEE Trans. Image Process.*, vol. 21, no. 2, pp. 517–526, Feb. 2012.
- [19] Q. Li and Z. Wang, "Reduced-reference image quality assessment using divisive normalization-based image representation," *IEEE J. Sel. Topics Signal Process.*, vol. 3, no. 2, pp. 202–211, Apr. 2009.
- [20] X. Gao, W. Lu, D. Tao, and X. Li, "Image quality assessment based on multiscale geometric analysis," *IEEE Trans. Image Process.*, vol. 18, no. 7, pp. 1409–1423, Jul. 2009.
- [21] Y. Liu, G. Zhai, X. Liu, and D. Zhao, "Perceptual image quality assessment combining free-energy principle and sparse representation," in *Proc. IEEE Int. Symp. Circuits Syst.*, 2016, pp. 1586–1589.
- [22] A. Mittal, A. K. Moorthy, and A. C. Bovik, "No-reference image quality assessment in the spatial domain," *IEEE Trans. Image Process.*, vol. 21, no. 12, pp. 4695–4708, Dec. 2012.
- [23] Y. Liu, K. Gu, S. Wang, D. Zhao, and W. Gao, "Blind quality assessment of camera images based on low-level and high-level statistical features," *IEEE Trans. Multimedia*, vol. 21, no. 1, pp. 135–146, Jan. 2019.
- [24] A. K. Moorthy and A. C. Bovik, "Blind image quality assessment: From natural scene statistics to perceptual quality," *IEEE Trans. Image Process.*, vol. 20, no. 12, pp. 3350–3364, Dec. 2011.
- [25] A. Mittal, R. Soundararajan, and A. C. Bovik, "Making a "completely blind" image quality analyzer," *IEEE Signal Process. Lett.*, vol. 20, no. 3, pp. 209–212, Mar. 2013.
- [26] L. Zhang, L. Zhang, and A. C. Bovik, "A feature-enriched completely blind image quality evaluator," *IEEE Trans. Image Process.*, vol. 24, no. 8, pp. 2579–2591, Aug. 2015.
- [27] J. Xu et al., "Blind image quality assessment based on high order statistics aggregation," *IEEE Trans. Image Process.*, vol. 25, no. 9, pp. 4444–4457, Sep. 2016.
- [28] Q. Wu, Z. Wang, and H. Li, "A highly efficient method for blind image quality assessment," in *Proc. IEEE Int. Conf. Image Process.*, 2015, pp. 339–343.
- [29] K. He, X. Zhang, S. Ren, and J. Sun, "Deep residual learning for image recognition," in *Proc. IEEE Conf. Comput. Vis. Pattern Recognit.*, 2016, pp. 770–778.
- [30] M. Tan, R. Pang, and Q. V. Le, "EfficientDet: Scalable and efficient object detection," in *Proc. IEEE Conf. Comput. Vis. Pattern Recognit.*, 2020, pp. 10781–10790.
- [31] C. Yu et al., "BiSeNet: Bilateral segmentation network for real-time semantic segmentation," in *Proc. Eur. Conf. Comput. Vis.*, 2018, pp. 325–341.
- [32] L. Kang, P. Ye, Y. Li, and D. Doermann, "Convolutional neural networks for no-reference image quality assessment," in *Proc. IEEE Conf. Comput. Vis. Pattern Recognit.*, 2014, pp. 1733–1740.
- [33] K. Ma et al., "dipiQ: Blind image quality assessment by learning-to-rank discriminable image pairs," *IEEE Trans. Image Process.*, vol. 26, no. 8, pp. 3951–3964, Aug. 2017.
- [34] J. Kim and S. Lee, "Fully deep blind image quality predictor," *IEEE J. Sel. Topics Signal Process.*, vol. 11, no. 1, pp. 206–220, Feb. 2017.
- [35] S. Bosse, D. Maniry, K. R. Müller, T. Wiegand, and W. Samek, "Deep neural networks for no-reference and full-reference image quality assessment," *IEEE Trans. Image Process.*, vol. 27, no. 1, pp. 206–219, Jan. 2018.
- [36] S. Su et al., "Blindly assess image quality in the wild guided by a self-adaptive hyper network," in *Proc. IEEE Conf. Comput. Vis. Pattern Recognit.*, 2020, pp. 3667–3676.
- [37] W. Zhang, K. Ma, G. Zhai, and X. Yang, "Uncertainty-aware blind image quality assessment in the laboratory and wild," *IEEE Trans. Image Process.*, vol. 30, pp. 3474–3486, 2021.
- [38] Y. Y. Schechner and N. Karpel, "Recovery of underwater visibility and structure by polarization analysis," *IEEE J. Ocean. Eng.*, vol. 30, no. 3, pp. 570–587, Jul. 2005.
- [39] M. Yang and A. Sowmya, "New image quality evaluation metric for underwater video," *IEEE Signal Process. Lett.*, vol. 21, no. 10, pp. 1215–1219, Oct. 2014.
- [40] Z. Li, Z. Gu, H. Zheng, B. Zheng, and J. Liu, "Underwater image sharpness assessment based on selective attenuation of color in the water," in *Proc. IEEE OCEANS*, 2016, pp. 1–4.
- [41] L. Li, "Underwater color image quality assessment," 2020. [Online]. Available: <https://github.com/LangtaoLi/Underwater-color-image-quality-assessment>
- [42] H. Lu et al., "Underwater image descattering and quality assessment," in *Proc. IEEE Int. Conf. Image Process.*, 2016, pp. 1998–2002.
- [43] S. Tang, C. Li, and Q. Tian, "Underwater image quality assessment based on human visual system," in *Proc. 13th Int. Congr. Image Signal Process. BioMed. Eng. Informat.*, 2020, pp. 378–382.
- [44] P. Guo, L. He, S. Liu, D. Zeng, and H. Liu, "Underwater image quality assessment: Subjective and objective methods," *IEEE Trans. Multimedia*, vol. 24, pp. 1980–1989, 2022.
- [45] P. Guo, H. Liu, D. Zeng, T. Xiang, L. Li, and K. Gu, "An underwater image quality assessment metric," *IEEE Trans. Multimedia*, pp. 1–14, 2022, doi: [10.1109/TMM.2022.3187212](https://doi.org/10.1109/TMM.2022.3187212).
- [46] Z. Wang, L. Shen, Z. Wang, Y. Lin, and Y. Jin, "Generation-based joint luminance-chrominance learning for underwater image quality assessment," *IEEE Trans. Circuits Syst. Video Technol.*, vol. 33, no. 3, pp. 1123–1139, Mar. 2023.
- [47] Z. Fu, X. Fu, Y. Huang, and X. Ding, "Twice mixing: A rank learning based quality assessment approach for underwater image enhancement," *Signal Process. Image Commun.*, vol. 102, 2022, Art. no. 116622.
- [48] C. Guo et al., "Underwater ranker: Learn which is better and how to be better," in *Proc. AAAI Conf. Artif. Intell.*, vol. 37, no. 1, pp. 702–709, 2023.
- [49] Z. Wang et al., "Domain adaptation for underwater image enhancement," *IEEE Trans. Image Process.*, vol. 32, pp. 1442–1457, 2023.
- [50] M. Li et al., "Human perceptual quality driven underwater image enhancement framework," *IEEE Trans. Geosci. Remote Sens.*, vol. 60, 2022, Art. no. 5634415.
- [51] F. Li, J. Wu, Y. Wang, Y. Zhao, and X. Zhang, "A color cast detection algorithm of robust performance," in *Proc. IEEE 5th Int. Conf. Adv. Comput. Intell.*, 2012, pp. 662–664.
- [52] K. Panetta, A. Samani, and S. Agaian, "Choosing the optimal spatial domain measure of enhancement for mammogram images," *J. Biomed. Imag.*, vol. 2014, pp. 1–8, 2014.
- [53] Y. Liu and X. Li, "No-reference quality assessment for contrast-distorted images," *IEEE Access*, vol. 8, pp. 84105–84115, 2020.

- [54] L. K. Choi, J. You, and A. C. Bovik, "Referenceless prediction of perceptual fog density and perceptual image defogging," *IEEE Trans. Image Process.*, vol. 24, no. 11, pp. 3888–3901, Nov. 2015.
- [55] A. Cohen, I. Daubechies, and J.-C. Feauveau, "Biorthogonal bases of compactly supported wavelets," *Commun. Pure Appl. Math.*, vol. 45, pp. 485–560, 1992.
- [56] K. Sharifi and A. Leon-Garcia, "Estimation of shape parameter for generalized Gaussian distributions in subband decompositions of video," *IEEE Trans. Circuits Syst. Video Technol.*, vol. 5, no. 1, pp. 52–56, Feb. 1995.
- [57] G. Zhai, A. Kaup, J. Wang, and X. Yang, "A dual-model approach to blind quality assessment of noisy images," in *Proc. Picture Coding Symp.*, 2013, pp. 29–32.
- [58] D. Zoran and Y. Weiss, "Scale invariance and noise in natural images," in *Proc. IEEE Int. Conf. Comput. Vis.*, 2009, pp. 2209–2216.
- [59] K. Gu, G. Zhai, X. Yang, and W. Zhang, "A new reduced-reference image quality assessment using structural degradation model," in *Proc. IEEE Int. Symp. Circuits Syst.*, 2013, pp. 1095–1098.
- [60] Y. Liu, K. Gu, X. Li, and Y. Zhang, "Blind image quality assessment by natural scene statistics and perceptual characteristics," *ACM Trans. Multimedia Comput. Commun. Appl.*, vol. 16, no. 3, pp. 1–91, 2020.
- [61] Q. Li, W. Lin, J. Xu, and Y. Fang, "Blind image quality assessment using statistical structural and luminance features," *IEEE Trans. Multimedia*, vol. 18, no. 12, pp. 2457–2469, Dec. 2016.
- [62] S. Ling et al., "Re-visiting discriminator for blind free-viewpoint image quality assessment," *IEEE Trans. Multimedia*, vol. 23, pp. 4245–4258, 2021.
- [63] C.-C. Chang and C.-J. Lin, "LIBSVM: A library for support vector machines," *ACM Trans. Intell. Syst. Technol.*, vol. 2, pp. 1–27, 2011. [Online]. Available: <http://www.csie.ntu.edu.tw/cjlin/libsvm>
- [64] K. Gu, G. Zhai, X. Yang, and W. Zhang, "Using free energy principle for blind image quality assessment," *IEEE Trans. Multimedia*, vol. 17, no. 1, pp. 50–63, Jan. 2015.
- [65] N. Venkatanath, D. Praneeth, M. C. Bh, S. S. Channappayya, and S. S. Medasani, "Blind image quality evaluation using perception based features," in *Proc. IEEE Nat. Conf. Commun.*, 2015, pp. 1–6.
- [66] C. Li et al., "An underwater image enhancement benchmark dataset and beyond," *IEEE Trans. Image Process.*, vol. 29, pp. 4376–4389, 2000.
- [67] A. M. Rohaly et al., "Final report from the video quality experts group on the validation of objective models of video quality assessment." Geneva, Switzerland: ITU-T Standards Contribution COM, 2000, pp. 9–80.



Jingchao Cao received the B.S. degree in electronic engineering from Xidian University, Xi'an, China, in 2014, and M.S. and Ph.D. degrees in computer science from the City University of Hong Kong, Hong Kong, in 2016 and 2022, respectively. He is currently a Lecturer in computer application technology with the Department of Computer Science and Technology, Ocean University of China, Qingdao, China. His research interests include computer vision, machine learning, image quality assessment, and image enhancement.



Shiqi Wang (Senior Member, IEEE) received the B.S. degree in computer science from the Harbin Institute of Technology, Harbin, China, in 2008, and the Ph.D. degree in computer application technology from Peking University, Beijing, China, in 2014. He is currently an Associate Professor with the Department of Computer Science, City University of Hong Kong, Hong Kong. He has authored more than 100 IEEE Transaction papers in the field of image processing and video coding. His research interests include image/video compression, analysis, and quality

assessment.



Guangtao Zhai (Senior Member, IEEE) received the B.E. and M.E. degrees from Shandong University, Shandong, China, in 2001 and 2004, respectively, and the Ph.D. degree from Shanghai Jiao Tong University, Shanghai, China, in 2009. He is currently a Research Professor with the Institute of Image Communication and Information Processing, Shanghai Jiao Tong University, Shanghai, China. His research interests include multimedia signal processing and perceptual signal processing. He was the recipient of the Award of National Excellent Ph.D. Thesis from the Ministry

of Education of China in 2012.



Yutao Liu received the B.S., M.S., and Ph.D. degrees in computer science from the Harbin Institute of Technology, Harbin, China, in 2011, 2013, and 2018, respectively. From 2018 to 2021, he was a Postdoctoral Fellow with Tsinghua University, Beijing, China. He is currently an Associate Professor with the Ocean University of China, Qingdao, China. His research interests include image quality assessment, image enhancement, and computer vision.



processing.

Junyu Dong (Member, IEEE) received the B.Sc. and M.Sc. degrees in applied mathematics from the Department of Applied Mathematics, Ocean University of China, Qingdao, China, in 1993 and 1999, respectively, and the Ph.D. degree in image processing from the Department of Computer Science, Heriot-Watt University, Edinburgh, U.K., in 2003. He is currently a Professor and the Head of the Department of Computer Science and Technology, Ocean University of China. His research interests include machine learning, big data, computer vision, and underwater image



Ke Gu (Senior Member, IEEE) is currently a Professor with the Beijing University of Technology, Beijing, China. His research interests include environmental perception, image processing, quality assessment, and machine learning. Dr. Gu was the recipient of the Best Paper Award from IEEE TRANSACTIONS ON MULTIMEDIA and the Best Student Paper Award at the IEEE International Conference on Multimedia and Expo (ICME) in 2016. He was the Leading Special Session Organizer in the IEEE International Conference on Visual Communications and Image Processing (VCIP) 2016 and the IEEE International Conference on Image Processing (ICIP) 2017. He is also an Associate Editor for *Computer Animation and Virtual Worlds* (CAVW) and *IET Image Processing* (IET-IPR), the Area Editor of *Signal Processing: Image Communication* (SPIC), and the Editor of *Applied Sciences, Displays, and Entropy*. He is also a reviewer for 20 top SCI journals.



Sam Kwong (Fellow, IEEE) received the B.S. degree in electrical engineering from the State University of New York, Buffalo, NY, USA, in 1983, and the M.S. degree in electrical engineering from the University of Waterloo, Waterloo, ON, Canada, in 1985, and the Ph.D. degree from the University of Hagen, North Rhine-Westphalia, Germany, in 1996. He is currently a Chair Professor with the Department of Computer Science, City University of Hong Kong, Hong Kong. His research interests include video coding, pattern recognition, and evolutionary algorithms. He was elevated to an IEEE fellow for his contributions on optimization techniques for cybernetics and video coding in 2014.